Nonvacuum, Maskless Fabrication of a Flexible Metal Grid Transparent Conductor by Low-Temperature Selective Laser Sintering of Nanoparticle Ink

Sukjoon Hong,[†,§] Junyeob Yeo,[†,§] Gunho Kim,[†] Dongkyu Kim,[†] Habeom Lee,[†] Jinhyeong Kwon,[†] Hyungman Lee,[†,‡] Phillip Lee,[†] and Seung Hwan Ko[†,*]

[†]Applied Nano Technology and Science Lab, Department of Mechanical Engineering, Korea Advanced Institute of Science and Technology (KAIST), 291 Daehak-ro, Yuseong-gu, Daejeon, 305-701, Korea, and [‡]Nano Sensor and Device Team, Korea Electronics Technology Institute (KETI), Gyeonggi-do, 463-816, Korea.
[§]J. Yeo and S. Hong contributed equally to this work.

ABSTRACT We introduce a facile approach to fabricate a metallic grid transparent conductor on a flexible substrate using selective laser sintering of metal nanoparticle ink. The metallic grid transparent conductors with high transmittance (>85%) and low sheet resistance (30 Ω/sq) are readily produced on glass and polymer substrates at large scale without any vacuum or high-temperature environment. Being a maskless direct writing method, the shape and the parameters of the grid can be easily changed by CAD data. The resultant metallic grid also showed a superior stability in terms of adhesion and bending. This transparent conductor is further applied to the touch screen panel, and it is confirmed that the final device operates firmly under continuous mechanical stress.

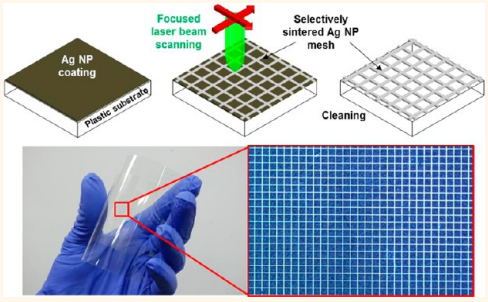

KEYWORDS: selective laser sintering · metal nanoparticle · transparent conductor · touch screen panel · flexible substrate

Transparent conductors are an inevitable component for various optoelectronics[1] such as LCDs,[2] OLED lighting,[3,4] photovoltaic cells,[5,6] and touch screen panels,[7,8] and their need is constantly growing for large-area flexible devices. To date, wide band gap transparent conductive oxides (TCO), indium tin oxide (ITO) in particular, have been the most widely used materials for transparent conductors due to their excellent optical transparency and low sheet resistance.[9] However, research on alternative materials for transparent conductors has been continuously increasing due to several drawbacks of ITO including its high scarcity, huge waste of target material,[10] and fragile nature,[11] which are adverse to next-generation electronics.

Possible alternatives for ITO are conducting polymers and carbon-based materials such as PEDOT:PSS,[12] graphene,[13] and CNT;[14] however, their performance highly depends on the sample preparation and often does not meet the requirements for many applications in terms of conductivity and stability.

Another class of transparent conductor comes from a regular metal grid[15,16] or random metal nanowire mesh,[5,17,18] which can theoretically exhibit electrical and optical properties even superior to ITO.[19] Recently, a metallic nanowire percolation network, using silver nanowires especially, has been intensively studied and presented excellent results in terms of transmittance and electrical conductivity.[8]

However, several drawbacks are reported for the nanowire-based transparent conductor. First, the performance of the resultant conducting film is very much dependent on the length of the nanowire, while the length is generally limited to <50 μm.[20] A method to elongate the length of the silver nanowire has been reported recently;[21] however, it makes the overall synthesis process more complicated and time-consuming. Second, the metallic nanowire percolation network

* Address correspondence to maxko@kaist.ac.kr.

Received for review January 27, 2013 and accepted May 28, 2013.

Published online June 03, 2013
10.1021/nn400432z

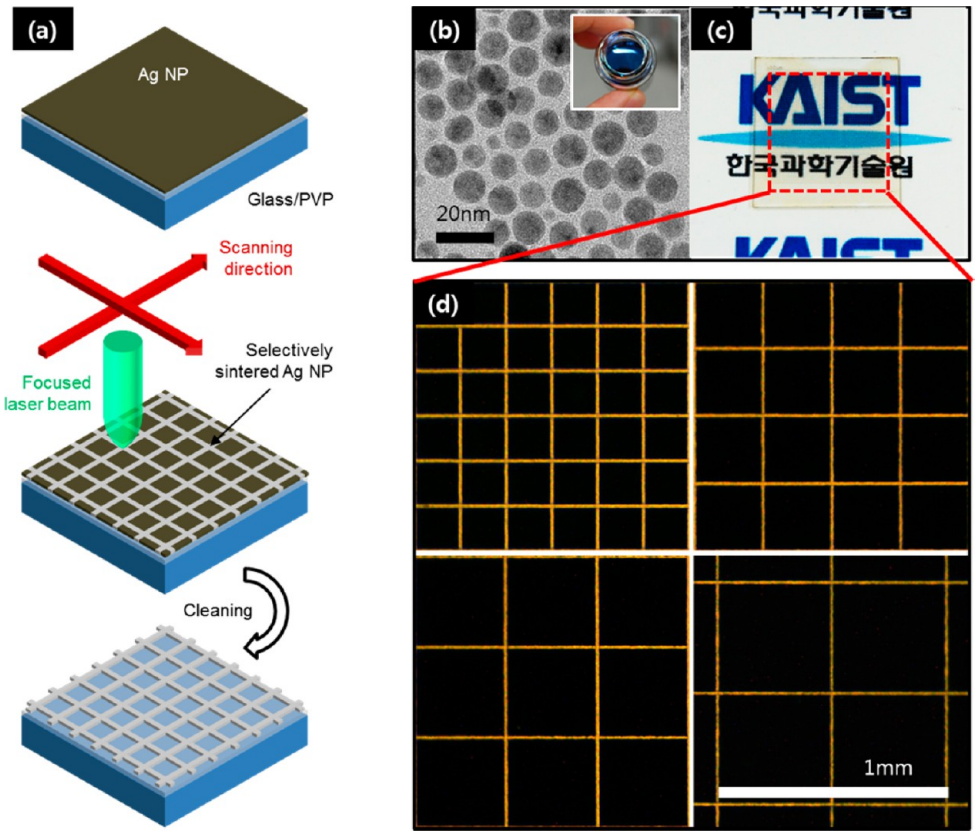

Figure 1. (a) Schematic diagram of selective laser sintering of Ag NPs for the fabrication of a transparent conductor. (b) TEM image of synthesized Ag NPs (inset: optical photograph of Ag NP ink). (c) Photograph of a transparent conductor on a glass substrate (metallic grid in the red-boxed region). (d) Optical stereoscope images of square-metallic grids at different grid sizes (200 to 500 μm, increment 100 μm).

cannot be utilized as-prepared, but requires an annealing process, either by bulk heating[17] or selective welding,[8] in order to remove the capping polymer around the nanowire and reduce the resistance at the junction. The metallic nanowire film is also vulnerable to scratching and can be easily detached from the substrate upon mild mechanical stress.[18]

In this paper, we introduce a novel approach to fabricate a metallic grid based transparent conductor without using any photolithography or metal vacuum deposition by direct selective laser sintering[23] of Ag nanoparticle (NP) ink, which has low sheet resistance and high transmittance on a large scale. By using a focused laser as a localized heat source, consistent silver conductor microlines are easily fabricated over a wafer-scale large area. Due to the direct writing method nature of the nanoparticle selective laser-sintering method,[22] the transmittance and the electrical conductivity can be easily tuned by changing the design of the metallic mesh by simply changing the CAD data without using any photomask for conventional photolithography. The process speed, compared to the inkjet-based process,[24] has been increased by 2−3 orders of magnitude by using a fast, electrically driven galvano-mirror. This process can be directly extended to a large-area, flexible substrate since it is conducted in a simple procedure without any vacuum environment, high temperature, or postprocessing, whereas the resultant transparent conductor also showed superior mechanical properties. A touch screen panel (TSP) is fabricated as a device demonstration and showed a stable performance under continuous mechanical stress.

Figure 1(a) illustrates the nonvacuum, maskless fabrication process of metal grid transparent conductor based on selective laser sintering of metal nanoparticles. For a typical experiment, Ag NP ink is first spin-coated on a glass substrate or polymer substrate where a thin layer of PVP (~100 nm) is coated in advance for the glass substrate to improve the adhesion between sintered Ag NPs and the substrate. An Nd:YAG laser operating in continuous-wave mode at 532 nm wavelength is then focused by a telecentric f-theta lens (f = 100 mm, Linos) at the Ag NP layer as a localized heat source to selectively convert the Ag NPs into a continuous conducting layer. The focused laser spot is rapidly scanned on the image plane by a laser scanner (HurrySCAN II, Scanlab) consisting of two electrically driven galvano-mirrors, where the detailed path and scanning speed of the spot are adjusted by a commercial computer-aided design (CAD) program (SAMLight) connected to the laser scanner. The residual Ag

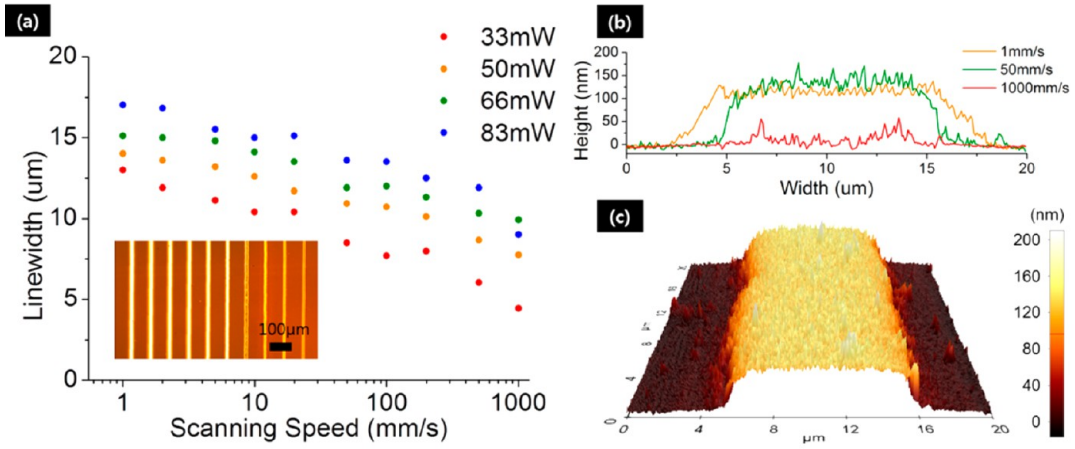

Figure 2. (a) Line width variation according to different laser scanning speed and laser power (inset, from left to right: optical image at 50 mW laser power at scanning speeds of 1, 2, 5, 10, 20, 50, 100, 200, 500, and 1000 mm/s, respectively). (b) Cross-section AFM profile at 50 mW laser power at different scanning speeds. (c) 3D profile by AFM of a single line at 50 mW laser power and 50 mm/s scanning speed.

NPs after the laser-sintering procedure can be easily removed by a short cleaning with toluene.

The Ag NPs used throughout the process are synthesized by following Korgel's method[25] with subtle modification. The synthesized Ag NPs are encapsulated by a self-assembled monolayer (SAM) to prevent further agglomeration at an average diameter of less than 10 nm, as can be confirmed from the TEM image shown in Figure 1(b). According to the Gibbs−Thomson equation, the processing temperature can be greatly reduced at such particle size due to the thermodynamic size effect. The detailed synthesis method can be found in the Materials and Methods section. The inset is the optical photograph of the resultant Ag NP ink, showing a dark bluish color with slight metallic hue.

RESULTS AND DISCUSSION

An example of a transparent conductor fabricated by this process is depicted in Figure 1(c), where the metallic grid is formed in the red-boxed region. We could observe that the sample after the cleaning procedure retains its transparency. Figure 1(d) is the microscope dark field images of square-shaped metal grid transparent conductors at different grid parameters, which are obtained by a stereoscope under the same magnification. The metal grids are successfully formed with continuous and consistent lines of the conductor. It also can be verified that the Ag NP layer subject to laser scanning recovers the properties of its bulk counterpart to be reflective, while all other Ag NPs are principally removed after washing from the substrate.

Selective laser sintering is basically a photothermal process, and thus the temperature distribution generated by the focused laser beam primarily determines the properties of the resultant conductor line. Either higher laser power or slower scanning speed naturally produces a broader line width, as the maximum temperature rise at the surface can be approximated to[26]

$$T_{\max}(z^* = 0) \cong \frac{\theta_c}{2\sqrt{\pi h_s^*}} \ln\left(\frac{16}{\xi v_s^{*2}}\right)$$

for relatively small scanning velocities with CW laser irradiation and surface absorption, where θ_c, h_s^*, ξ, and V_s^* correspond to the (normalized) laser power, thickness of the film, a constant, and the scanning speed, respectively. The line widths of the conducting line produced by a single scanning at different scanning speeds (1−1000 mm/s) and laser powers (33−83 mW) are plotted in Figure 2(a). The measured line widths mostly lie between 10 and 15 μm, and this range is reasonably in accord with the laser beam diameter ($1/e^2$) for Gaussian illumination, which is estimated to be ~10 μm for the current optical settings.

The inset of Figure 2(a) is the optical image of the laser-sintered NP conductor line set corresponding to the 50 mW laser power in the graph. At low laser scanning speeds, the lines are highly reflective but with rather blurred edges. The edge profile becomes sharper as the scanning speed increases, yet the reflectance drops abruptly when the scanning speed exceeds a certain threshold value, which is ~100 mm/s for this specific configuration.

These features can be explained in the conductor cross-section profiles measured by atomic force microscope (AFM) images, as shown in Figure 2(b). The conductor line sidewall angle at 1 mm/s scanning speed is considerably smaller than that of the line scanned at 50 mm/s. This is probably due to increased heat diffusion at lower laser scanning speed. This smaller sidewall angle requires more transition width from the conductor line, which contributes to a wider blurred edge in the optical image. At the speed of 1000 mm/s, the height is apparently lower than the other ones mainly because of the insufficient laser

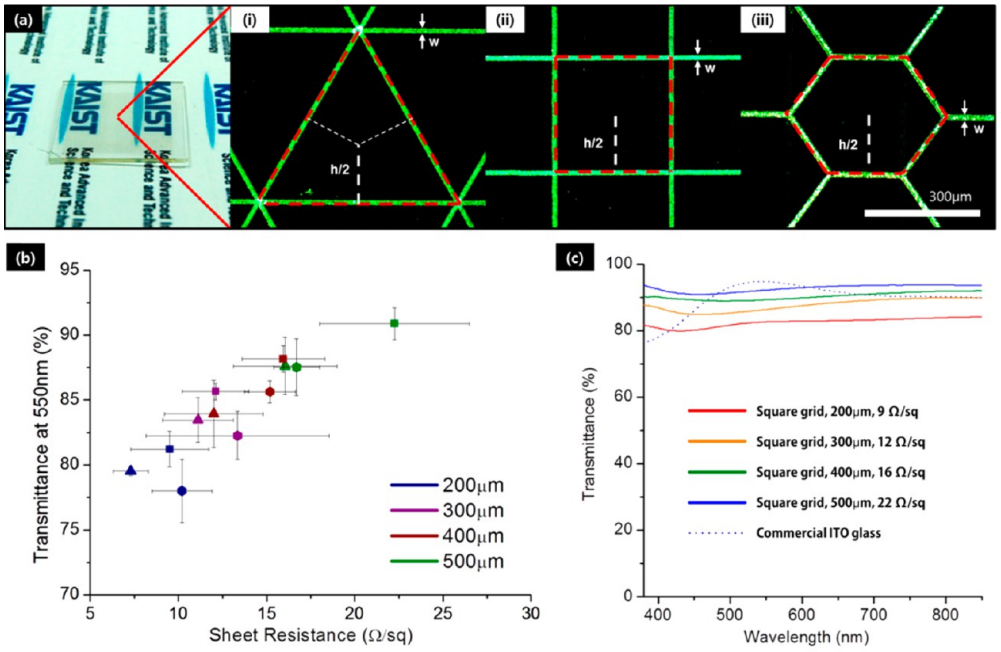

Figure 3. (a) Optical images of (i) square, (ii) triangle, and (iii) hexagonal shaped grids (h = 300 μm). (b) Transmission at 550 nm and sheet resistance at different grid sizes (the shape of each point on the graph corresponds to the grid shape). (c) Transmission spectrum at different square-shaped grid sizes.

irradiation for complete NP sintering. Therefore, the scanning speed around 50 mm/s is supposed to be the most favorable for the current application, yet the lasing parameters such as wavelength, spot size, power, and scanning speed have to be reoptimized for different NP sintering conditions including NP ink composition and coating thickness.

In addition, it is noticeable that the cross-section profile at 1000 mm/s has a volcano-like shape with a rim of ~7 μm diameter, which is supposed to arise from the Marangoni flow of the NP ink from the center to the ridge through the temperature gradient or thermocapillarity. This rim structure is quite uniformly created along the scanned line at high scanning speed and responsible for the highly sharp edge in the optical image. Such thorny structures around the rim generated in the NP sintering process can be found in the previous research as well.[27]

Figure 2(c) shows a typical AFM 3D profile of a laser-sintered NP conductor at 50 mW and 50 mm/s that has a nearly rectangular shape with a height of ~130 nm at ~11 μm width. Its cross-section is uniform throughout the line except for some defects such as dust from uncontrolled environments. The resistivity of the laser-sintered NP conductor is found to be ~7 $\mu\Omega$ cm, which is calculated from $R = \rho l/A$ where l and A are the length and the cross-section of a single line. This resistivity is only a few times higher than the resistivity of bulk silver (ρ = 1.59 $\mu\Omega$ cm)[28] probably due to the nanopores generated in the sintered metal conductor due to residual solvent and SAM trapped inside, but still low enough to be applied as a fine electrical conductor.

As a direct writing process, an arbitrary metal pattern can be fabricated by selective laser sintering without any premade conventional photomask or vacuum deposition. The maskless nature of the current process could allow easy pattern design modification by simple CAD data change. Therefore, a systematic parametric design study to find the optimum transparent grid conductor could be easily performed without making so many sets of photomasks. Three types of grids (triangular, square, and hexagonal) with 3- or 4-fold rotation symmetry are considered as grid shapes for a transparent conductor whose geometry is characterized by the apothem $h/2$ of the holes, as shown in the optical images in Figure 3(a). The width w has been fixed to ~12 μm, as all lines are drawn at the same sintering condition (50 mW, 20 mm/s), while h is changed from 200 to 500 μm with 100 μm increment. For the measurement of sheet resistance and transmittance, five distinct samples are fabricated for each combination of grid shape and size on a 2 cm × 2 cm area. Its sheet resistance and transmittance are measured by the two-terminal method and a UV−vis spectrophotometer (Jasco V530), respectively, and plotted in Figure 3(b), where each error bar covers five different values measured from separate samples. The transmittance at 550 nm wavelength is indicated as representative data for transparency.

Although the criteria for choosing transparent conductors vary among different applications,[9] sheet resistance lower than 30 Ω/sq and transmittance higher than 85% are repeatedly achieved by this process for the grid size beyond 300 μm. Different grid shapes

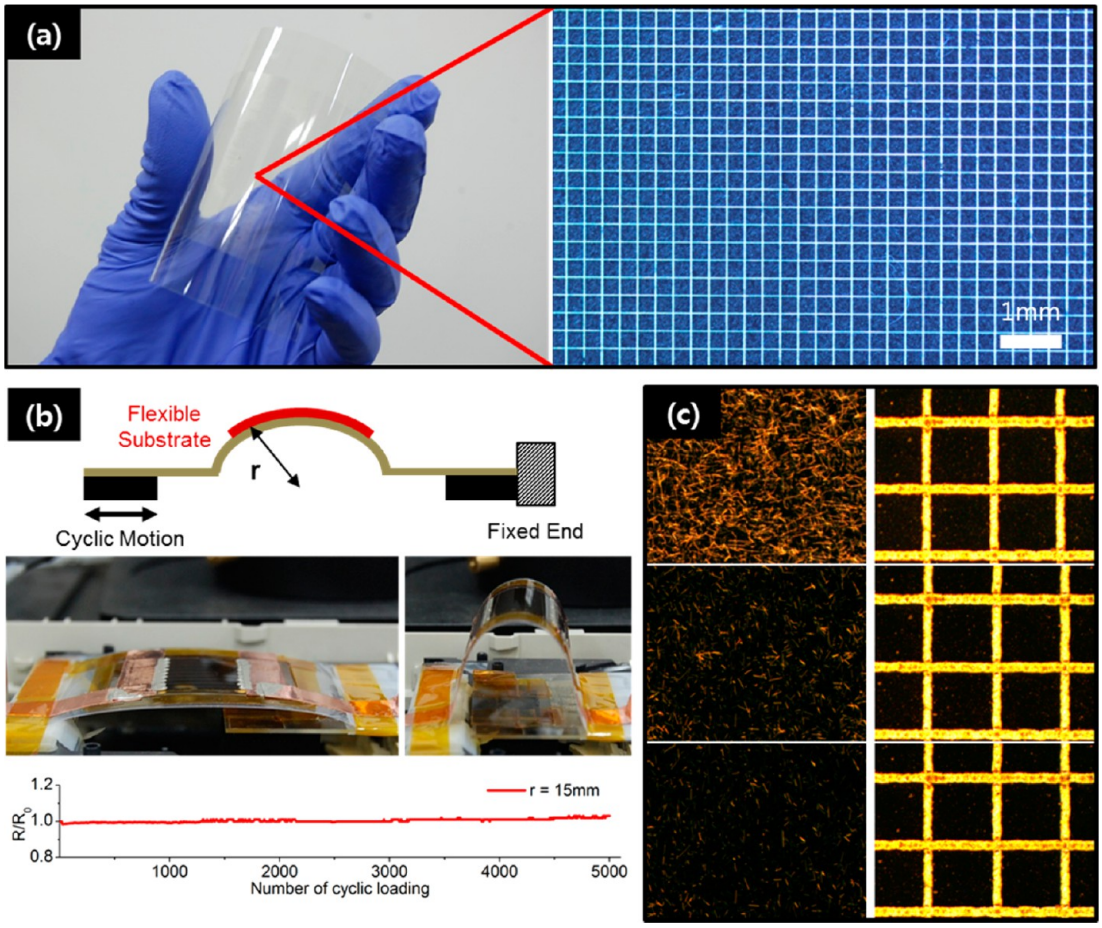

Figure 4. (a) Transparent conductor fabricated on a flexible (PEN) substrate (metallic grid on a 5 cm × 5 cm region). (b) Test setup of cyclic bending, photograph of minimum and maximum bending deformation of the sample carrier of a flexible substrate, and resistance change according to the number of cyclic bending. (c) Optical image of a transparent conductor made of Ag NW mesh (left column) and Ag NP sintering (right column) as-prepared (first row), after first adhesive tape test (second row), and after second adhesive tape test (third row).

appear to yield different sheet resistance and transmittance; however, they are supposed to be the same regardless of the grid shape for $w \ll h$ theoretically.[29] A potential reason for these variances is the galvanomirror, which rotates mechanically and is subject to different acceleration and deceleration according to the grid shape and the scanning path. The stability of this process can be further improved by controlling the environment including the temperature, humidity, and neglected parameters such as solvent drying conditions after the spin-coating procedure. The effect of line width and height on the transmittance and the sheet resistance is shown in the Supporting Information (see Supporting Figure S1).

Figure 3(c) is the transmittance spectrum of a square-shaped grid measured from 380 to 850 nm, where the dotted line represents a commercial high-transmittance ITO for comparison. We can verify that the transmittance of a metallic grid fabricated by this process can be as high as an ITO-based transparent conductor, for the UV region in particular. Further improvement in the transmittance is yet achievable by focusing the laser beam more tightly with a lens having a higher NA.

Basically selective laser sintering is a low-temperature metal patterning process, and it can be directly applied to a flexible substrate because the area subject to the elevated temperature is highly localized due to the reduced heat-affected zone. Figure 4(a) shows a square-shaped metal transparent conductor grid of 300 μm size fabricated at the scanning speed of 100 mm/s on a PEN substrate (Teonex, 125 μm thick, DuPont), whose glass transition temperature (T_g) is as low as 120 °C. No observable damage on the substrate is found after a complete process (see Supporting Figure S2). The sheet resistance is measured to be 36.6 Ω/sq for a 5 cm × 5 cm sample and 23.3 Ω/sq for a 2 cm × 2 cm sample, showing that the resistivity of the Ag electrode on a polymer substrate can closely approach the one fabricated on a glass substrate through careful alignment of the optical system. It is also noteworthy that the total processing time required for the scanning of a metallic grid on a 5 cm × 5 cm area is less than 3 min, demonstrating that this

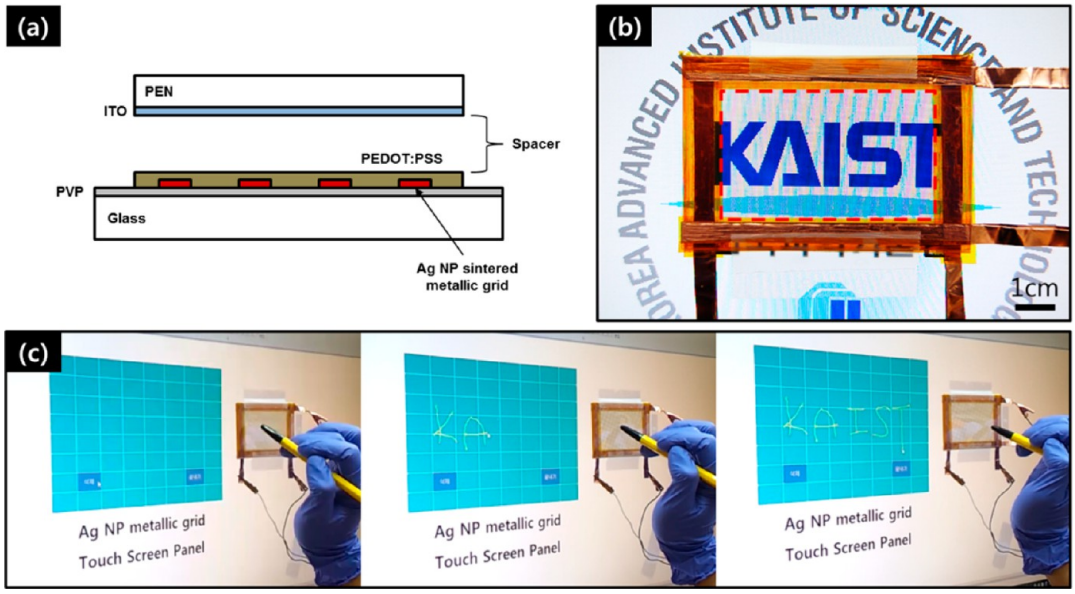

Figure 5. (a) Schematic diagram of a touch screen panel (TSP) fabricated on a metallic grid. (b) TSP on an LCD screen. (c) Demonstration of applying a metallic grid transparent conductor for a touch panel by writing the letters "KAIST" using the fabricated TSP.

process is applicable for large-area, fast fabrication as well.

The electrical and mechanical stability of the NP laser sintered grid transparent conductor is further tested under cyclic bending deformation and the adhesive tape test. The experimental setup for the cyclic bending deformation is shown in Figure 4(b). The bending of the flexible substrate is created by moving one end at the frequency of 1 Hz while the other end is fixed, yielding a radius of curvature r = 15 mm at the maximum bending deformation. Fifty conductor lines with l = 30 mm are fabricated on the PI substrate (Upilex, 125 μm thick, Ube Industries) and connected to two copper electrodes with silver paste for the *in situ* measurement of resistance (see Supporting Figure S3 for a detailed outline of the sample used for the bending test). Throughout 5000 bending cycles, the change in resistance was within 3% of its original value (from 26.2 Ω to 27.0 Ω), where the increase probably arises from the contact resistance between the sintered lines and the electrode.

A usual adhesive tape test is performed on a square-shaped grid, whereas the same test is conducted on a Ag nanowire based transparent conductor for comparison. The left column in Figure 4(c) shows that a large part of Ag NW mesh is removed from the substrate after two consecutive adhesive tape tests. On the contrary, the Ag NP based metal grid transparent conductor in the right column shows almost negligible change in its morphology, showing that the NP laser sintering process enhances not only the adhesion between individual Ag NPs but also the adhesion between sintered Ag pattern and the substrate. The improvement in adhesion is confirmed on the polymer substrates as well (see Supporting Figure S4). The variation in the resistance is also measured to be insignificant for a number of adhesion tests for both rigid and flexible substrates. Such mechanical robustness is particularly beneficial for the device that operates under continuous mechanical stress.

As a device demonstration, a square-shaped metallic grid is applied for the rigid transparent conductor in a four-wire analogue resistive touch panel, whose structure is shown in Figure 5(a). The size of each grid is 300 μm, where the total area covered by the grid is 6.5 cm × 5 cm. A thin layer of PEDOT:PSS is deposited on top of the metallic grid as a protecting conductor layer. For the other side, ITO-PEN film (Peccell, PECF-IP, 15 Ω/sq) is selected to be used as a counter electrode with a comparable sheet resistance. A commercial copper tape is used as the electrical lines that apply the voltage across each conductor. Figure 5(b) shows the corresponding TSP on the LCD screen, and its active area is denoted by the red dotted box. We can verify that the TSP preserves the transparency so that the image on the LCD screen is apparent through the device. The TSP is connected to a commercial controller, and its performance is confirmed by writing the letters "KAIST" on the screen, as shown in Figure 5(c). (For a video of the TSP operating, see the Supporting Information.)

CONCLUSION

In summary, we have demonstrated a metallic grid based transparent conductor that is fabricated by selective laser sintering of Ag NP ink that is conducted without vacuum deposition or conventional photomasks at plastic-compatible low temperature. As a

local heat source to convert NPs into conductor grid lines, the focused laser beam is scanned over the wafer scale and conductor lines of ~130 nm height and ~11 μm width are readily produced. As a direct writing method, the transparent grid conductor pattern can be easily adjusted by a CAD program, and three different types of metal grids (triangle, square, and hexagonal) of 200 to 500 μm size are fabricated without any premade mask. Their performance is comparable to ITO, yielding a transmittance higher than 85% and a sheet resistance of less than 30 Ω/sq at a grid size of >300 μm. This process can be directly extended to a large-area flexible substrate, as confirmed by the metallic grid fabricated on a PEN substrate over a 5 cm × 5 cm area. The conductor lines produced by the laser sintering on the glass and flexible substrate also showed an excellent stability in terms of adhesion and bending. The resultant transparent conductor is applied to TSP as the device demonstration, and the final device operated steadily under continuous mechanical stress.

MATERIALS AND METHODS

Ag NP Ink Preparation for SLS Process. The synthesis of Ag NPs is based on the method reported by Korgel et al.[25] A 0.20 M tetroactylammonium bromide ($(C_8H_{17})_4NBr$) solution is mixed with 20.4 mL of chloroform and added to 30 mM $AgNO_3$ in 30 mL of DI water in order to form a two-phase system. The solution is stirred vigorously for 1 h, and 0.16 mg of long-chain thiol (dodecanethiol ($C_{12}H_{25}SH$)) is added to the solution while stirring. After 15 min, 0.43 M aqueous sodium borohydride ($NaBH_4$) in 24 mL of DI water is added into the organic phase as a reducing agent to nucleate nanocrystals. The solution is kept at room temperature for 3.5 h. Chloroform is then removed with a rotary evaporator, and the remaining particles are washed with ethanol and acetone to remove phase transfer catalyst, excessive thiol, and other byproducts. The resultant Ag NPs are suspended in toluene or alphaterpineol at 10 wt %.

Conflict of Interest: The authors declare no competing financial interest.

Acknowledgment. This work is supported by National Research Foundation of Korea (NRF) (grant nos. 2012-0008779, 2012-0003722), Global Frontier R&D Program on Center for Multiscale Energy System (grant no. 2012-054172) funded by the Ministry of Science, ICT & Future, the Cooperative R&D Program (grant no. B551179-10-01-00) on the Korea Research Council Industrial Science and Technology, and the Technology Development Program (grant no. SL122685) funded by the Small & Medium Business Administration, Korea.

Supporting Information Available: Sheet resistance and transmittance of a metal grid transparent conductor at different line widths and heights, AFM profile of PEN substrate with a sintered Ag electrode and after selective etching of the electrode, detailed outline of the metal pattern used in the bending test, and optical microscope image before and after the adhesive tape test on various substrates are provided in a pdf file. The operation of metal grid transparent conductor based TSP is provided as a video clip. This material is available free of charge *via* the Internet at http://pubs.acs.org.

REFERENCES AND NOTES

1. Hecht, D. S.; Hu, L.; Irvin, G. Emerging Transparent Electrodes Based on Thin Films of Carbon Nanotubes, Graphene, and Metallic Nanostructures. *Adv. Mater.* **2011**, *23*, 1482–1513.
2. Blake, P.; Brimicombe, P. D.; Nair, R. R.; Booth, T. J.; Jiang, D.; Schedin, F.; Ponomarenko, L. A.; Morozov, S. V.; Gleeson, H. F.; Hill, E. W.; *et al*. Graphene-Based Liquid Crystal Device. *Nano Lett.* **2008**, *8*, 1704–1708.
3. Wu, J.; Agrawal, M.; Becerril, H. A.; Bao, Z.; Liu, Z.; Chen, Y.; Peumans, P. Organic Light-Emitting Diodes on Solution-Processed Graphene Transparent Electrodes. *ACS Nano* **2009**, *4*, 43–48.
4. Tak, Y.-H.; Kim, K.-B.; Park, H.-G.; Lee, K.-H.; Lee, J.-R. Criteria for ITO (Indium−Tin-Oxide) Thin Film as the Bottom Electrode of an Organic Light Emitting Diode. *Thin Solid Films* **2002**, *411*, 12–16.
5. Yang, L.; Zhang, T.; Zhou, H.; Price, S. C.; Wiley, B. J.; You, W. Solution-Processed Flexible Polymer Solar Cells with Silver Nanowire Electrodes. *ACS Appl. Mater. Interfaces* **2011**, *3*, 4075–4084.
6. Yu, Z.; Li, L.; Zhang, Q.; Hu, W.; Pei, Q. Silver Nanowire-Polymer Composite Electrodes for Efficient Polymer Solar Cells. *Adv. Mater.* **2011**, *23*, 4453–4457.
7. Wang, J.; Liang, M.; Fang, Y.; Qiu, T.; Zhang, J.; Zhi, L. Rod-Coating: Towards Large-Area Fabrication of Uniform Reduced Graphene Oxide Films for Flexible Touch Screens. *Adv. Mater.* **2012**, *24*, 2874–2878.
8. Lee, J.; Lee, P.; Lee, H.; Lee, D.; Lee, S. S.; Ko, S. H. Very Long Ag Nanowire Synthesis and Its Application in a Highly Transparent, Conductive and Flexible Metal Electrode Touch Panel. *Nanoscale* **2012**, *4*, 6408–6414.
9. Gordon, R. G. Criteria for Choosing Transparent Conductors. *MRS Bull.* **2000**, *25*, 52–57.
10. Green, M. A. Estimates of Te and In Prices from Direct Mining of Known Ores. *Prog. Photovoltaics: Res. Appl.* **2009**, *17*, 347–359.
11. Cairns, D. R.; Witte, R. P., II; Sparacin, D. K.; Sachsman, S. M.; Paine, D. C.; Crawford, G. P.; Newton, R. R. Strain-Dependent Electrical Resistance of Tin-Doped Indium Oxide on Polymer Substrates. *Appl. Phys. Lett.* **2000**, *76*, 1425–1427.
12. Elschner, A.; Lövenich, W. Solution-Deposited PEDOT for Transparent Conductive Applications. *MRS Bull.* **2011**, *36*, 794–798.
13. Kim, K. S.; Zhao, Y.; Jang, H.; Lee, S. Y.; Kim, J. M.; Kim, K. S.; Ahn, J.-H.; Kim, P.; Choi, J.-Y.; Hong, B. H. Large-Scale Pattern Growth of Graphene Films for Stretchable Transparent Electrodes. *Nature* **2009**, *457*, 706–710.
14. Gruner, G. Carbon Nanotube Films for Transparent and Plastic Electronics. *J. Mater. Chem.* **2006**, *16*, 3533–3539.
15. van de Groep, J.; Spinelli, P.; Polman, A. Transparent Conducting Silver Nanowire Networks. *Nano Lett.* **2012**, *12*, 3138–3144.
16. Zou, J.; Yip, H.-L.; Hau, S. K.; Jen, A. K. Y. Metal Grid/Conducting Polymer Hybrid Transparent Electrode for Inverted Polymer Solar Cells. *Appl. Phys. Lett.* **2010**, *96*, 203301/1–203301/3.
17. Hu, L.; Kim, H. S.; Lee, J.-Y.; Peumans, P.; Cui, Y. Scalable Coating and Properties of Transparent, Flexible, Silver Nanowire Electrodes. *ACS Nano* **2010**, *4*, 2955–2963.
18. Zeng, X.-Y.; Zhang, Q.-K.; Yu, R.-M.; Lu, C.-Z. A New Transparent Conductor: Silver Nanowire Film Buried at the Surface of a Transparent Polymer. *Adv. Mater.* **2010**, *22*, 4484–4488.
19. Lee, J.-Y.; Connor, S. T.; Cui, Y.; Peumans, P. Solution-Processed Metal Nanowire Mesh Transparent Electrodes. *Nano Lett.* **2008**, *8*, 689–692.
20. Sun, Y.; Yin, Y.; Mayers, B. T.; Herricks, T.; Xia, Y. Uniform Silver Nanowires Synthesis by Reducing $AgNO_3$ with Ethylene Glycol in the Presence of Seeds and Poly(vinyl pyrrolidone). *Chem. Mater.* **2002**, *14*, 4736–4745.
21. Lee, J. H.; Lee, P.; Lee, D.; Lee, S. S.; Ko, S. H. Large-Scale Synthesis and Characterization of Very Long Silver Nanowires via Successive Multistep Growth. *Cryst. Growth Des.* **2012**, *12*, 5598–5605.

22. Ko, S. H.; Pan, H.; Grigoropoulos, C. P.; Luscombe, C. K.; Frechet, J. M. J.; Poulikakos, D. All-Inkjet-Printed Flexible Electronics Fabrication on a Polymer Substrate by Low-Temperature High-Resolution Selective Laser Sintering of Metal Nanoparticles. *Nanotechnology* **2007**, *18*, 345202.
23. Son, Y.; Yeo, J.; Moon, H.; Lim, T. W.; Hong, S.; Nam, K. H.; Yoo, S.; Grigoropoulos, C. P.; Yang, D.-Y.; Ko, S. H. Nanoscale Electronics: Digital Fabrication by Direct Femtosecond Laser Processing of Metal Nanoparticles. *Adv. Mater.* **2011**, *23*, 3176–3181.
24. Ahn, B. Y.; Lorang, D. J.; Lewis, J. A. Transparent Conductive Grids via Direct Writing of Silver Nanoparticle Inks. *Nanoscale* **2011**, *3*, 2700–2702.
25. Korgel, B. A.; Fitzmaurice, D. Self-Assembly of Silver Nanocrystals into Two-Dimensional Nanowire Arrays. *Adv. Mater.* **1998**, *10*, 661–665.
26. Bauerle, D. *Laser Processing and Chemistry*, 4th ed.; Springer: Berlin, Germany, 2011; Chapter 9.
27. Chung, J.; Ko, S.; Bieri, N. R.; Grigoropoulos, C. P.; Poulikakos, D. Conductor Microstructures by Laser Curing of Printed Gold Nanoparticle Ink. *Appl. Phys. Lett.* **2004**, *84*, 801–803.
28. Yeo, J.; Hong, S.; Lee, D.; Hotz, N.; Lee, M.-T.; Grigoropoulos, C. P.; Ko, S. H. Next Generation Non-Vacuum, Maskless, Low Temperature Nanoparticle Ink Laser Digital Direct Metal Patterning for a Large Area Flexible Electronics. *PLoS One* **2012**, *7*, e42315.
29. Neyts, K.; Real, A.; Marescaux, M.; Mladenovski, S.; Beeckman, J. Conductor Grid Optimization for Luminance Loss Reduction in Organic Light Emitting Diodes. *J. Appl. Phys.* **2008**, *103*, 093113/1–093113/5.